RESEARCH ARTICLE-MECHANICAL ENGINEERING

An Magnetohydrodynamics Effect of Non-Newtonian Fluid Flows Over a Stretching/Shrinking Surface with CNT

K. N. Sneha[1] · U. S. Mahabaleshwar[1] · K. M. Nihaal[1] · H. F. Oztop[2,3,4]

Abstract
In this study, carbon nanotubes, which serve as nanoparticles, are added to the basic fluid. By using a similarity transformation, the governing equations are converted into a set of ordinary differential equations (ODEs), which are then solved analytically. In order to simulate the flow and heat transfer behavior of carbon nanotubes, the Prandtl numbers for water and kerosene are 6.72 and 21, respectively. The precision of the analytical solution found in this study for the nonlinear flow of fluid containing carbon nanotubes is what makes it so beautiful. With the available experimental data, the proposed model is reliable. The main physical parameters for the Jeffrey fluid flow on the stretching/shrinking surface using carbon nanotubes are shown in tables and graphs and described in detail for the thermal and boundary layers. Carbon nanotubes enhance the heat more than the nanofluid; for this purpose, the work on carbon nanotubes flow through stretching/shrinking surfaces has many applications in biomedical, solar energy, generator cooling, nuclear system cooling, etc. Therefore, it is quite significant to assimilate the analytical extension of heat transfer fluid in the presence of magnetohydrodynamics under the influence of slip velocity. Further, carbon nanotubes can effectively elucidate the base materials' thermal performance and mechanical properties. Here, we assimilated the extension of heat transfer fluid in the incidence of magnetohydrodynamics under the influence of slip velocity analytically. Further, carbon nanotubes can successfully elucidate the base materials' thermal performance and mechanical properties.

Keywords Jeffrey fluid flow · Magnetohydrodynamics · Slip velocity · Carbon nanotubes · Stretching/shrinking

List of Symbols

B_0 (A/m)	Magnetic field
c, b	Constants
C_p (m² s⁻² K⁻¹)	Specific heat
d	Stretching/shrinking coefficient
C_f	Skin friction

k (kg ms⁻³ K^{-1})	Thermal conductivity
k^* (m⁻¹)	Absorption coefficient
L_1, L_2	Slip parameter
Nu	Nusselt number
Pr	Prandtl number
Q	Chandrasekhar number
q_r (W m⁻²)	Radiation heat flux
Rd	Radiation parameter
T (K)	Temperature
T_w (K)	Wall temperature
T_∞ (K)	Ambient temperature
V_c	Mass transpiration
u, v (ms⁻¹)	Velocity complements
x, y (m)	Coordinate axis

✉ K. M. Nihaal
  nihaal.kmdvg@gmail.com

✉ H. F. Oztop
  hfoztop1@gmail.com

1 Department of Studies in Mathematics, Davangere University, Shivagangothri, Davangere 577 007, India

2 Department of Mechanical and Nuclear Engineering, College of Engineering, University of Sharjah, 27272 Sharjah, United Arab Emirates

3 Department of Mechanical Engineering, Technology Faculty, Fırat University, Elazig, Turkey

4 Department of Medical Research, China Medical University Hospital, China Medical University, Taichung, Taiwan

Greek symbols

α (m² s⁻¹)	Thermal diffusivity
β	Deborah number
Λ	Stagnation parameter

χ_1	Relaxation ratio
χ_2	Retardation time
η	Similarity variable
ν	Kinematic viscosity
μ	Dynamic viscosity
ρ	Density
τ	Inclined angle
σ	Electrical conductivity
$\sigma*$	Stefan–Boltzmann constant
$\Gamma_1, \ \Gamma_2$	First-order and second-order slip parameters
λ	Solution domain
τ_w	Wall heat flux
q_w	Surface heat flux
$\varepsilon_1, \varepsilon_2, \varepsilon_3, \varepsilon_4$	Constants

Subscripts

f	Base fluid
nf	Nanofluid
CNT	Carbon nanotube

1 Introduction

One of the fundamental components of nanotechnology is nanofluid, which is a possible heat transfer fluid. Carbon nanotubes are used in boiler exhaust flue gas recovery, nuclear systems cooling, engine transmission oil, electronic cooling, high power lasers, biomedical applications, polymer extraction, and fiber equipment, and in a cooling bath, crystals develop and cool on infinite metallic plates, lubrications, drilling, and solar water heating. These are some of the many applications of carbon nanotubes.

Carbon nanotubes (CNTs) based nanofluid as a heat transfer system. Carbon nanotubes are a commonly used fullerene allotrope with a lengthy and cylindrical chemical structure made up of sheets of graphite. There are two categories of CNTs, SWCNTs, and MWCNTs. The thermophysical properties of carbon nanotubes are subservient along with graphene sheets getting aligned consecutively within the tube, which results in this kind of material executing the properties of metal or semiconductor explored by Waqar et al. [1]. Iijima [2] explores the chemical process and heat radiation effect on nanofluid flow, which relies on time along with changing fluid characteristics. Baughman et al. [3] investigated the heat transmission with magnetohydrodynamics and the flow of carbon nanotube suspensions of nanoparticles over a stretching sheet (linear).

The study of the (magnetohydrodynamics) electrically conductive fluid flow driven by a stretched sheet is essential in modern metallurgy applications, plastic sheet drawings, metal-working processes, and so on. In each of these techniques, a cooling speed has a significant impact on the final product's condition. Sarpakaya was the first to investigate the flow of magnetohydrodynamics in this specific case. The Jeffrey fluid model is preferred in several cases since convicted derivatives are replaced with time derivatives. The multi-phase flow of the Jeffrey fluid was investigated by Nazeer et al. [4] within a magnetized horizontal surface. A numerical investigation of the effects of activation energy and microorganisms on a Jeffrey nanofluid squeezing flow contained by two parallel disks using a chemical process was done by Chu et al. [5]. Abbas et al. [6] examined Darcy Forchheimer's electromagnetic stretched flow of carbon nanotubes across an inclined cylinder while taking entropy optimization and quartic chemical reaction into account. Hayat et al. [7] present heat transfer and boundary layer flow in a nanoparticle-enhanced Jeffrey fluid. Turkyilmazoglu [8], in his paper, considered parallel external flow to explore Jeffrey fluid flow with heat transfer. In the latter, which included several physical parameters, exact solutions of the linear or exponential systems were provided. With the aid of the Brinkman model, Mahabaleshwar et al. [9] investigated the behavior of velocity profiles due to slip parameters in Newtonian liquid flow over shrinking /stretching sheets in the penetrable media. Mahabaleshwar et al. [10] explored Newtonian fluid flow and the magnetohydrodynamics effect caused by a superlinear stretched sheet. Siddheshwar et al. [11] conducted an analytical study on the magnetohydrodynamics flow across a stretched sheet of a viscoelastic fluid embedded in a porous media.

Mahabaleshwar et al. [12] contributed to the inclined magnetohydrodynamics effect, thermal radiation effects, and Stefan blowing effects on Newtonian fluids. Siddheshwar et al. [13] presented a new perspective approach for a nonlinear boundary layer that arises in stretched surface problems with non-Newtonian/Newtonian liquids. Ramesh et al. [14, 15] used a semi-infinite flat sheet to investigate a precise remedy for 2D viscous boundary layer flow along with the magnetic effect. Mahantesh et al. [16] proposed the second-order slip flow across a stretched surface with heat transfer. Mahabaleshwar [17, 18] investigated a new exact solution for the flow of a fluid through porous media for a variety of boundary conditions. An investigation of electrically conducting viscoelastic fluid flow over a porous media barrier that is linearly expanded [19–21]. Anuar et al. [22] studied the heat transfer of carbon nanotubes over an exponentially stretching/shrinking sheet with a suction and slip effect. Anwar et al. [23] investigated the unsteady magnetohydrodynamics flow of Jeffery fluid flow with wall velocity and Newtonian fluid. Fluid flow and heat transfer of carbon nanotubes along with a flat plate with a Navier slip boundary were investigated by

Khan et al. [24]. Shalini et al. [25] studied the unsteady magnetohydrodynamics chemically reacting mixed convection nanofluids flow past an inclined pours stretching sheet with slip effect and variable thermal radiation and heat source. The effects of inclined Lorentz force and thermal radiation on natural convection inside a porous container with a micropolar nano liquid and an elliptical tilted heater are investigated by Yana et al. [26]. Unsteady MHD flow for Casson fluid with porous media with stretching/shrinking plate with mass transpiration and Brinkman ratio is investigated by Anusha et al. [27, 28]. Mahabaleshwar [29] investigated the inclined Lorentz force and Schmidt number on chemically reactive Newtonian fluid flow on a stretchable surface when Stefan blowing and thermal radiation are significant. Thermal management for conjugate heat transfer of curved solid conductive panel coupled with different cooling systems using non-Newtonian power law nanofluid applicable to photovoltaic panel systems. The recent works related to MHD and porous media can be found in these studies [30–34].

Further, the effects of carbon nanotube-based nanofluids on mass transpiration, radiation, and the inclined field of magnetism in the presence of Jeffery fluid flow are discussed. The discussion is established over a stretching/shrinking sheet. Furthermore, the velocity profiles, skin friction, and heat transfer on the plate are examined to discuss the effect that the different physical governing parameters, such as the Prandtl number, or the magnetic field, have on them, and to introduce the consequences of the physical parameters imposed on the velocity profiles.

The main purpose and motivation of this paper is to address the magnetohydrodynamics effect on fluid flow over a stretching surface in the presence of CNTs. Using these CNTs, the present problem is examined with the help of analytical results. The main reason to accompany CNTs is due to its extraordinary electrical and heat conductivity properties. The complimentary error function was utilized to get a solution for temperature profile. The organization of the present work is to provide the new results on carbon nanotubes and examine these results in the analytical approach.

The first section includes an introduction, and in Sect. 2, the physical model and solution are discussed; Sect. 3 comprises results and a discussion of the graphical representation, and the conclusions of the current study are presented in Sect. 4.

2 Physical Model and Solution

In a water/oil-based nanofluid containing both single- and multi-wall carbon nanotubes, consider two-dimensional flows over a flat plate with heat transfer. The stretching/shrinking sheet is parallel to the $y = 0$ plane. The flow is induced by a stretching/shrinking sheet caused by the simultaneous application of two equal and opposite forces along the x-axis. A uniform surface heat flux is applied to the plate surface. It is assumed that the flow is laminar, continuous, and incompressible. Thermal equilibrium is considered between the base fluid and the carbon nanotubes [35–37].

$$\frac{\partial u}{\partial x} + \frac{\partial v}{\partial y} = 0, \tag{1}$$

$$
u\frac{\partial u}{\partial x} + v\frac{\partial u}{\partial y} = u_e \frac{\partial u_e}{\partial x}
$$
$$
+ \frac{v_{nf}}{(\chi_1 + 1)} \left[\frac{\partial^2 u}{\partial y^2} + \chi_2 \left(u\frac{\partial^3 u}{\partial x \partial y^2} + v\frac{\partial^3 u}{\partial y^3} - \frac{\partial^2 u}{\partial y^2}\frac{\partial u}{\partial x} + \frac{\partial^2 u}{\partial x \partial y}\frac{\partial u}{\partial y} \right) \right]
$$
$$
- \frac{\sigma_{nf} B_0^2}{\rho_{nf}} \mathrm{Sin}^2(\tau)(u - u_e), \tag{2}
$$

$$\left(\rho C_{\mathrm{p}}\right)_{nf}\left(v\frac{\partial T}{\partial y} + u\frac{\partial T}{\partial x} \right) = k_{nf}\frac{\partial^2 T}{\partial y^2} - \frac{\partial q_{\mathrm{r}}}{\partial y}. \tag{3}$$

Here, (u, v) stand for (x, y) directional velocity components correspondingly, $U_{\mathrm{w}}(x)$ is surface velocity, χ_1 is the relaxation ratio, χ_2 denotes retardation time, effective kinematic viscosity v_{nf}, T is temperature, and $\left(\rho C_{\mathrm{p}}\right)_{nf}$ and k_{nf} denotes heat capacity and thermal conductivity, respectively. The following are effective nanofluid properties with base fluid containing a solid volume fraction of the CNTs: [38]

$$
\left.
\begin{aligned}
&v_{nf} = \frac{\mu_{nf}}{\rho_{nf}}, \quad \rho_{nf} = \phi\rho_{\mathrm{CNT}} + \rho_f(1 - \phi), \\
&\alpha_{nf} = \frac{\kappa_{nf}}{(\rho C_p)_{nf}}, \quad (\rho C_p)_{nf} = (\rho C_p)_f(1 - \phi) + (\rho C_p)_{\mathrm{CNT}}\phi, \\
&\frac{\sigma_{nf}}{\sigma_f} = 1 - \frac{3\phi\left(1 - \frac{\sigma_{\mathrm{CNT}}}{\sigma_f}\right)}{\frac{\sigma_{\mathrm{CNT}}}{\sigma_f} - 2 + \left(1 - \frac{\sigma_{\mathrm{CNT}}}{\sigma_f}\right)\phi}, \\
&\frac{k_{nf}}{k_f} = \frac{2\phi\frac{k_{\mathrm{CNT}}}{k_{\mathrm{CNT}} - \kappa_f}\log\frac{k_f + k_{\mathrm{CNT}}}{2\kappa_f} + 1 - \phi}{1 + 2\phi\frac{k_f}{k_{\mathrm{CNT}} - k_f}\log\frac{k_{\mathrm{CNT}} + k_f}{2k_f} - \phi}.
\end{aligned}
\right\} \tag{4}
$$

Using [37] diffusion approximation, the radiative heat flux is determined by Mahabaleshwar et al. [29]:

$$q_r = -\frac{16\sigma^*}{3k^*}T_\infty^3\frac{\partial T}{\partial y}, \tag{5}$$

where, k^* and σ^* is the mean absorption coefficient and Stefan–Boltzmann constant, respectively. The Taylor's series expansion of the term T^4 being a linear function of temperature is expressed as follows by Mahabaleshwar et al. [29]:

$$T^4 = T_\infty^4 + 4(T - T_\infty)T_\infty^4 + \ldots \tag{6}$$

Omitting high-order terms in Eq. (6) leaving the initial term in $(T - T_\infty)$, T^4 can be estimated by:

$$T^4 \cong 4TT_\infty^3 - 3T_\infty^4, \tag{7}$$

Employing Eqs. (6–7), Eq. (3) can be rewritten as,

$$v\frac{\partial T}{\partial y} + u\frac{\partial T}{\partial x} = \frac{k_{nf}}{(\rho C_\text{p})_{nf}}\left(1 + \frac{16T_\infty^3 \sigma^*}{3k^*k_{nf}}\right)\frac{\partial^2 T}{\partial y^2}. \tag{8}$$

2.1 Boundary Conditions

With the boundary conditions

$$\left.\begin{array}{l} u = U_w(x) = dcx + \Gamma_1\dfrac{\partial u}{\partial y} + \Gamma_2\dfrac{\partial^2 u}{\partial y^2}, \\[2mm] v = v_w, \quad T = T_w(x), \end{array}\right\} \text{ at } y = 0$$

$$\left.\begin{array}{l} u \to u_e(x) = xa, \quad \dfrac{\partial u}{\partial y} \to 0, \quad T \to T_\infty. \end{array}\right\} \text{at y} \to \infty \tag{9}$$

where Γ_1 and Γ_2 are first-order and second-order slip parameters, following suitable similarity variables are introduced as follows:

$$\eta = \sqrt{\frac{c(\gamma_1 + 1)}{v_f}}\, y, \quad u = xcf_\eta(\eta),$$

$$v = -\sqrt{\frac{v_f c}{(1 + \gamma_1)}}f(\eta), \quad \theta = \frac{T - T_\infty}{T_w - T_\infty}, \tag{10}$$

$$T_w(x) = T_\infty + bx,$$

The transformed Eqs. (2–3) and (8) are expressed as follows:

$$f_{\eta\eta\eta}\varepsilon_3 + ff_{\eta\eta} - (f_\eta)^2 - \varepsilon_3\beta\left(ff_{\eta\eta\eta\eta} - (f_{\eta\eta})^2\right) + \Lambda^2$$
$$- (f_\eta - \Lambda)\frac{\varepsilon_1}{\varepsilon_2}Q\text{Sin}^2(\tau) = 0,$$

$$\left(\varepsilon_5 + \frac{4}{3}Rd\right)\theta_{\eta\eta} + \text{Pr}\,\varepsilon_4 f\theta_\eta = 0,$$

$$\left(\varepsilon_5 + \frac{4}{3}Rd\right)\theta_{\eta\eta} + \text{Pr}\,\varepsilon_4\left(f\theta_\eta - f_\eta\theta\right) = 0. \tag{11}$$

The renovated boundary limitations

$$f(0) = V_c, \quad f_\eta(0) = L_1 f_{\eta\eta}(0) + L_2 f_{\eta\eta\eta}(0) + d,$$
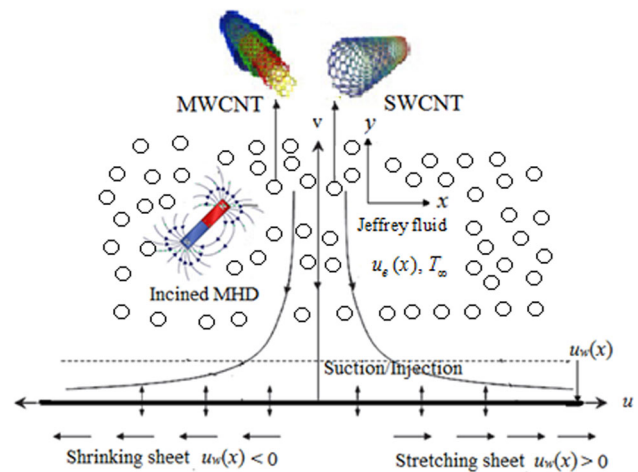$$\theta(0) = 1, \quad f_\eta(\infty) = \Lambda, \quad f_{\eta\eta}(\infty) = 0\ \theta(\infty) = 0. \tag{12}$$

Fig. 1 Geometry of the flow

Here, $\Lambda = \frac{a}{c}$ is a stagnation parameter, Prandtl number $\text{Pr} = \frac{v_f}{\alpha}$, L_1 and L_2 the slip parameter, β Deborah number, and wall transpiration $v_w = -\sqrt{\frac{cv_f}{1+\gamma_1}}$, Q Chandrasekhar number. Hence, the boundaries are the governing boundaries in the Jeffery fluid flow.

The major physical dimensionless parameters like skin friction coefficient Cf_x and Nusselt number Nu_x are well-stated as,

$$Cf_x = \frac{\tau_w}{\rho_{nf}u_e^2(x)}, \tag{13}$$

$$Nu_x = \frac{xq_w}{(T_w - T_\infty)\alpha}. \tag{14}$$

where,

$$\tau_w = \mu_{nf}\left(\frac{\partial u}{\partial y}\right)\bigg|_{y=0}, \quad q_w = -\alpha_{nf}\left(\frac{\partial T}{\partial y}\right)\bigg|_{y=0}.$$

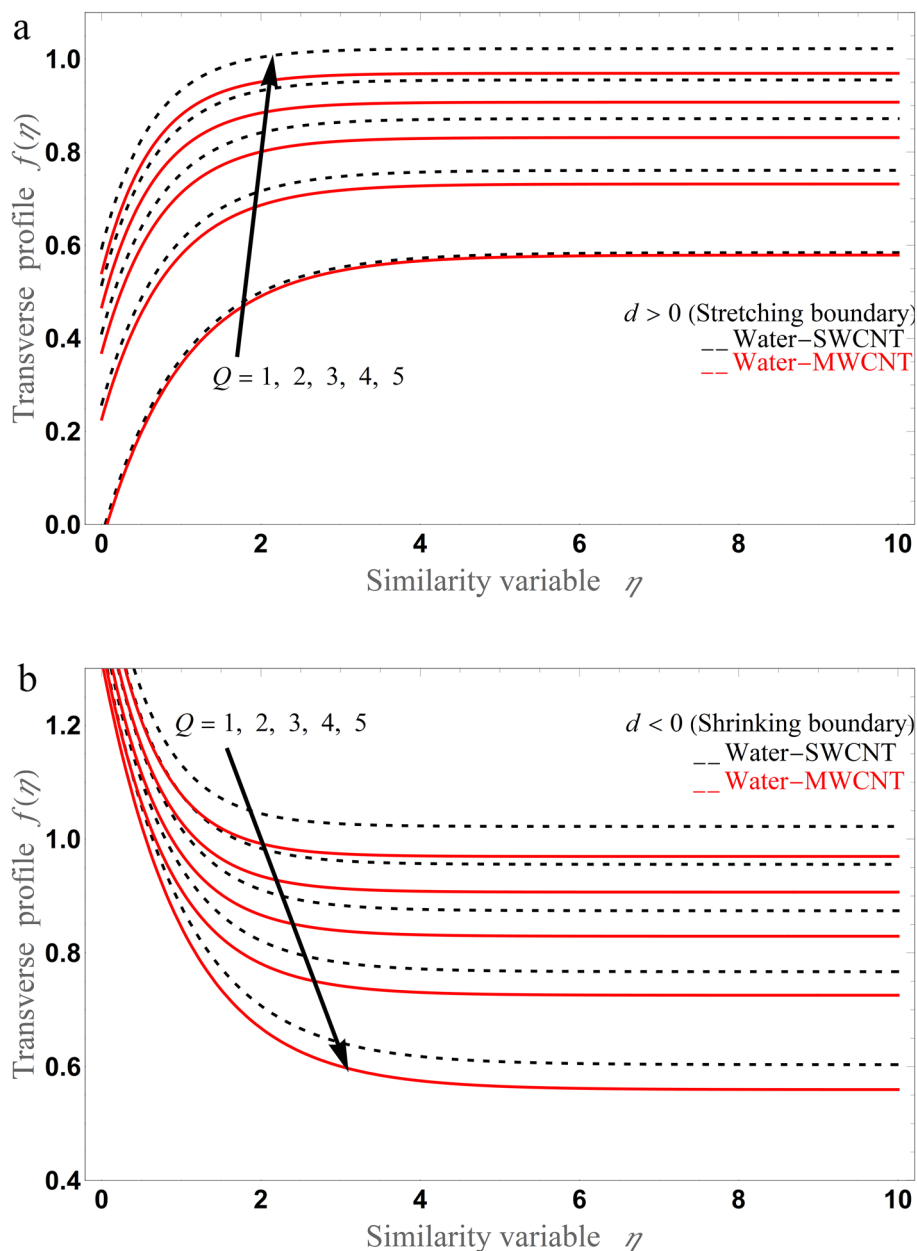We get Eq. (15) after applying the similarity transformation Eq. (10)

$$Cf_x\,\text{Re}_x^{1/2} = \varepsilon_3\,f_{\eta\eta}(0), \quad Nu_x\,\text{Re}_x^{-1/2} = -\frac{\varepsilon_4}{\varepsilon_5}\theta_\eta(0). \tag{15}$$

2.2 Solution of Momentum Problem

Our examination is fundamentally founded on classical Crane's solution $f(\eta) = 1 - exp(-\lambda\eta)$,

[39]. Here, $V_c = Q = \beta = \Lambda = L_1 = L_2 = 0$ in the most basic flow condition as a consequence, and we can execute an explanation of the procedure for the general case

Fig. 2 **a** Curves of transverse profile for different values of Q. **b** Curves of transverse for various values of Q

As a consequence, the form and number of solutions will be determined by the polynomial roots (17).
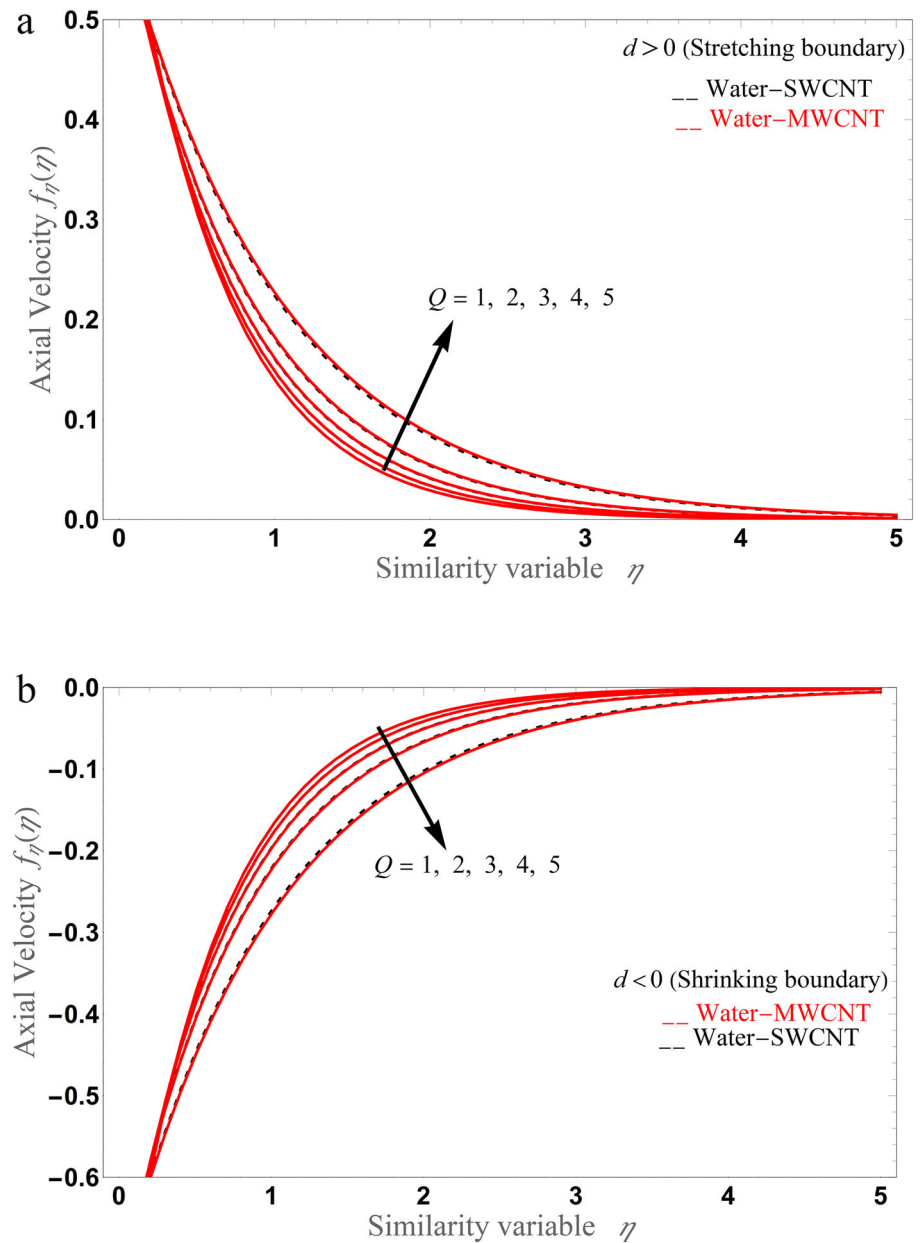
For the specific case, $\Lambda = 0$, (12) converts

$$f(\eta) = V_c + \Lambda\eta + \frac{d - \Lambda}{\lambda(1 + L_1\lambda + L_2\lambda^2)}(1 - exp(-\lambda\eta)) \quad (16)$$

We get the mathematical equation relating the actual boundaries by substituting Eq. (11) first of (16)

$$(d - \Lambda)\left\{ \begin{array}{l} (1 + L_1\lambda + L_2\lambda^2)\left[-\frac{\varepsilon_1}{\varepsilon_2}Q\mathrm{Sin}^2(\tau) + \lambda\left(\varepsilon_3\lambda - V_c + \varepsilon_3\beta V_c\lambda^2\right)\right] + d\left(-1 + \varepsilon_3\beta\lambda^2\right) \\ -\Lambda - 2\Lambda L_1\lambda + 2\Lambda L_2\lambda^2 - \varepsilon_3\beta\Lambda\lambda^2 + \eta\Lambda\lambda\left(1 + L_1\lambda + L_2\lambda^2\right)\left(-1 + \varepsilon_3\beta\lambda^2\right) \end{array} \right\}. \quad (17)$$

Fig. 3 a Impact of Chandrasekhar number on velocity profile for stretching sheet. **b** Impact of Chandrasekhar number on velocity profile for shrinking sheet

$$\left(\varepsilon_3 \beta \lambda^2 - 1\right) d(1 + L_1\lambda + L_2\lambda^2)$$

$$+ \left(-\frac{\varepsilon_1}{\varepsilon_2}Q\mathrm{Sin}^2\tau + \lambda\left(\varepsilon_3\lambda - V_c + \varepsilon_3\beta V_c\lambda^2\right)\right) \tag{18}$$

$$= 0$$

Provided the reduced form Eqs. (11) and the energy Eq. (15), a further solution can be found supposing linear wall temperature.

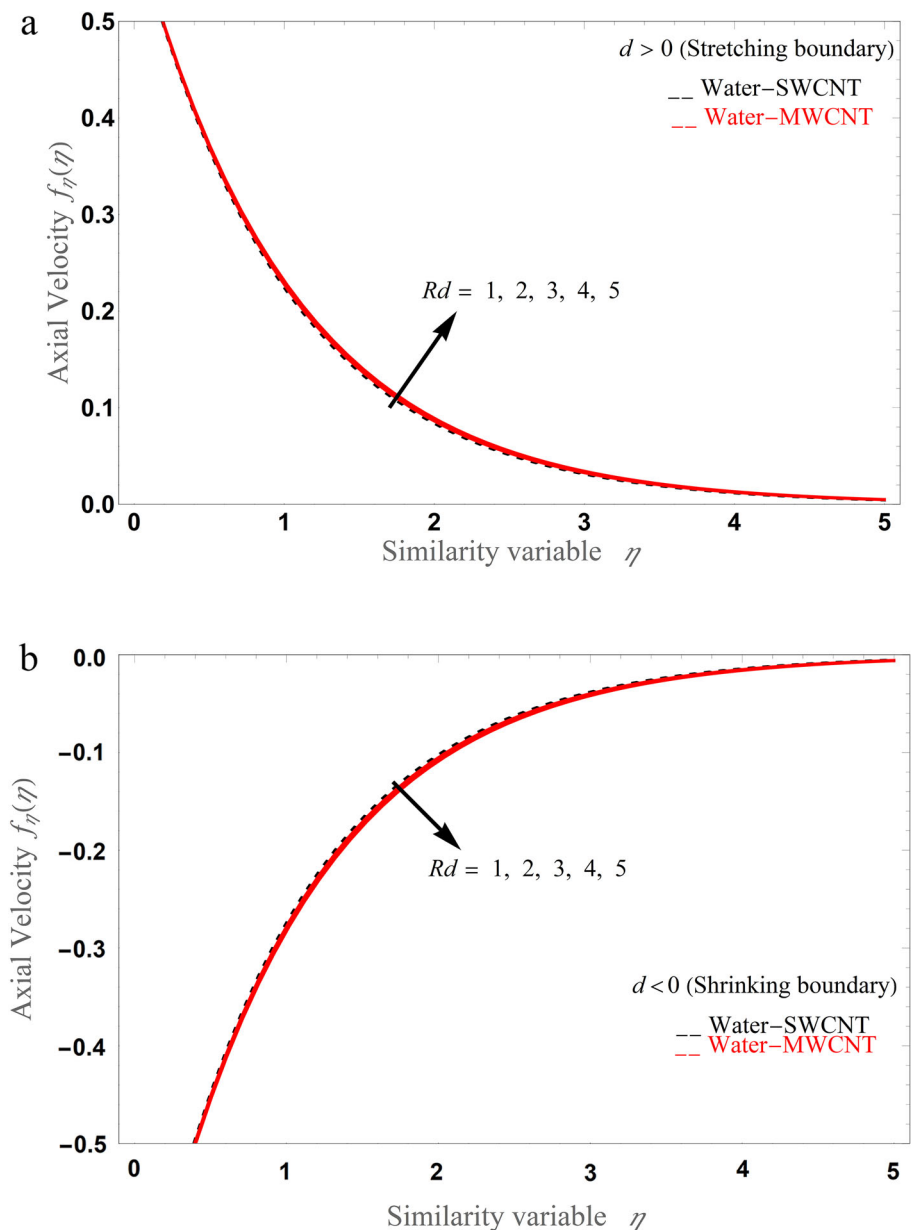### 2.3 Solution of Energy Problem

$$\theta = exp(-\lambda\eta), \tag{19}$$

that produces

$$d\,\mathrm{Pr}\,\varepsilon_4 + \left[\mathrm{Pr}\,\varepsilon_4 V_c - \lambda\left(\varepsilon_5 + \frac{4}{3}Rd\right)\lambda(1 + L_1\lambda + L_2\lambda^2)\right] = 0, \tag{20}$$

It is simple to get between (18) and (20).

Fig. 4 a Impact of radiation on velocity profile for stretching sheet. **b** Impact of radiation on velocity profile for shrinking sheet
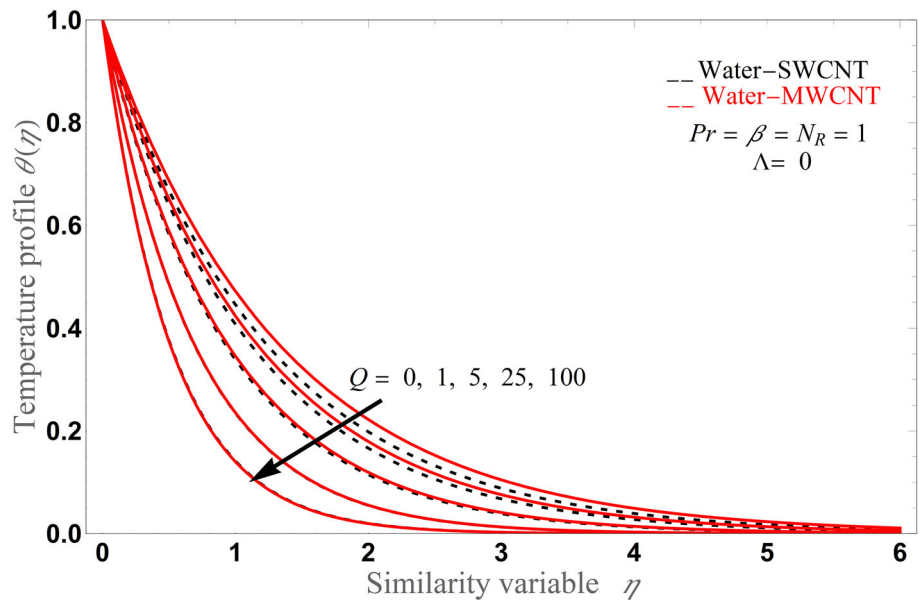

$$\lambda = \sqrt{\frac{\left(\varepsilon_5 + \frac{4}{3}Rd\right) - \mathrm{Pr}\,\varepsilon_4\varepsilon_3 \pm \sqrt{\left(\left(\varepsilon_5 + \frac{4}{3}Rd\right) - \mathrm{Pr}\,\varepsilon_4\varepsilon_3\right)^2 + 4\,\mathrm{Pr}\,\beta\frac{\varepsilon_1\varepsilon_4\varepsilon_3}{\varepsilon_2}Q\mathrm{Sin}^2\tau\left(\varepsilon_5 + \frac{4}{3}Rd\right)}}{2\beta\varepsilon_3\left(\varepsilon_5 + \frac{4}{3}Rd\right)}}, \tag{21}$$

$$V_c = \frac{\lambda\left(\varepsilon_5 + \frac{4}{3}Rd\right)}{\mathrm{Pr}\,\varepsilon_4} - \frac{d}{\lambda(1 + L_1\lambda + L_2\lambda^2)}.$$

As a consequence, one can get

$$\left. \begin{array}{l} f(\eta) = V_c + \dfrac{d - \Lambda}{\lambda(1 + L_1\lambda + L_2\lambda^2)}(1 - Exp[-\lambda\eta]), \\[2mm] \theta = Exp[-\lambda\eta]. \end{array} \right\} \tag{22}$$

Fig. 5 Impact of Q on the temperature profile

Temperature is unaffected by these parameters because λ is independent of L_1, L_2 and D. The corresponding suction parameter V_c, on the other hand, will change as these parameters change.

After that, the physically interesting parameters are determined.

$$-f_{\eta\eta}(\eta) = \frac{(d-\Lambda)\lambda}{(1+L_1\lambda+L_2\lambda^2)}, \quad -\theta_\eta(0) = \lambda. \tag{23}$$

As a consequence, on expanding the slip parameter, the coefficient of skin friction, and variations in wall shear and Nusselt number, just as velocity and temperature distributions, the Jeffrey fluid will evolve to f in the case of $\Lambda = 1$ as well as $d = 1$. $f(\eta) = V_c + \eta$ any Q,L_1, L_2, V_c and λ are real. A temperature solution is also given when these two variables are added together.

$$\theta(\eta) = \frac{Erfc\left[\sqrt{\frac{Pr\varepsilon_4}{2\left(\varepsilon_5+\frac{4}{3}Rd\right)}}(V_c+\eta)\right]}{Erfc\left[\sqrt{\frac{Pr\varepsilon_4}{2\left(\varepsilon_5+\frac{4}{3}Rd\right)}}\,V_c\right]}, \tag{24}$$

The complementary error function is denoted by *Erfc*. As a result, we obtain the same expression.

$$-\theta_\eta(0) = \frac{-\sqrt{\frac{2}{\pi}}\sqrt{\frac{Pr\varepsilon_4}{\left(\varepsilon_5+\frac{4}{3}Rd\right)}}Exp\left[-\frac{Pr}{\left(\varepsilon_5+\frac{4}{3}Rd\right)}\right]}{Erfc\left[\sqrt{\frac{Pr\varepsilon_4}{2\left(\varepsilon_5+\frac{4}{3}Rd\right)}}\,V_c\right]}. \tag{25}$$

3 Result and Discussion

The Jeffery fluid flow known as non-Newtonian flows with heat transfer is analytic and steady. A comprehensive mathematical model of the carbon nano-multi-wall carbon nanotube-based nano-liquids due to stretching/shrinking sheets with radiations has been presented in this research paper. The systems of PDEs Eqs. (1), (2), and (3) are transformed into a set of nonlinear ODEs via similarity variables. The exact analytical solution is investigated the different combinations of physical parameters viz. Exact analytical explanations for velocity and energy profiles can be achieved by using the appropriate similarity variable. As a result of the multiple graphs that will be presented and discussed below on the subject, we now understand the technology involved in such fascinating dynamics. Furthermore, similar visuals provide a comparison of the transverse, axial, and temperature profiles of single-wall carbon nanotubes and multi-wall carbon nanotubes, for which the solid volume fraction will be fixed, with dashed and solid lines indicating the solutions for single-wall carbon nanotubes and multi-wall carbon nanotubes, respectively (Fig. 1). A comparison of the present study and existing works by other authors is illustrated in Table 1.

Figures 2, 3 depict the axial and transverse velocity versus similarity variables for different entities of Chandrasekhar's number's Q. In Fig. 2a, b with fixed $Pr = 6.2$ for base fluid water for single-wall carbon nanotubes and multi-wall carbon nanotubes, it is identified that the velocity field increases for the raise of the different values of Chandrasekhar's number's Q. As one can see, $f(\eta)$ increases as Chandrasekhar's number's Q also rises, and, for the suction case, the boundary layer thickness is shifted away from the x-axis. It is similarly noticed that $f_\eta(\eta)$ improves water and kerosene oil

Fig. 6 Impact of Q on the temperature profile
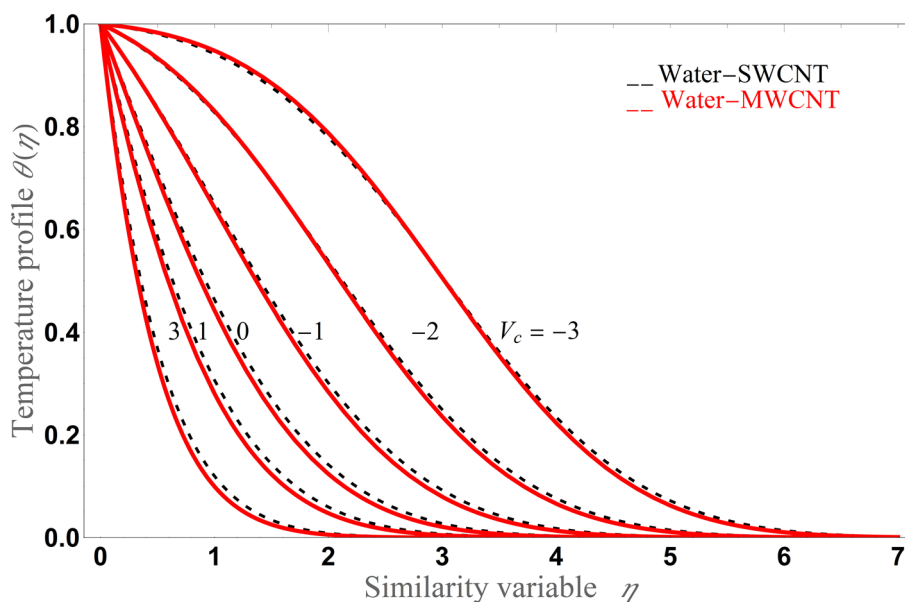
**Fig. 7** Nusselt number versus mass transpiration V_c for stretched sheet
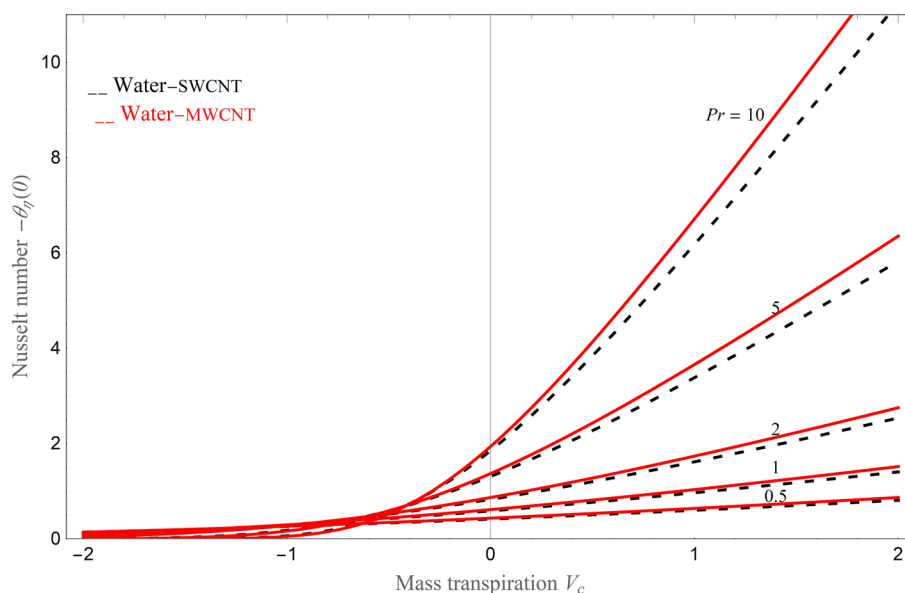
nano-liquid for multi-wall carbon nanotubes as compared with single-wall carbon nanotubes. Figure 3a,b illustrates the effect of Chandrasekhar's number's Q on $f_\eta(\eta)$, for large estimates of the Chandrasekhar's number's Q, velocity $f_\eta(\eta)$ and its related boundary layer decrease. Chandrasekhar's numbers affect the extent of the boundary layer thickness, which decreases in a stretching/shrinking surface when the parameter Q increases.

The action of the radiation parameter R_d on $f_\eta(\eta)$ is depicted in Fig. 4a, b. The velocity profile for SWCNTs and MWCNTs using base liquid water indicates a reduction in the behavior of the radiation parameter. The consequence of the radiation field is to develop the stretching sheet and reduction it for the sheet with shrinking. The radiation parameter affects the extent of the boundary layer thickness, which

decreases in a stretching/shrinking surface when the parameter Q increases.

Figure 5 portrays the effect of the temperature profile and raise of Chandrasekhar's number's Q for both single-wall carbon nanotubes and multi-wall carbon nanotubes. For higher values of Chandrasekhar's number's Q, the temperature distribution and associated boundary layer thickness decrease. It is observed that the temperature and boundary layer density rise in SWCNTs and MWCNTs when the volume fraction increases and the boundary layer thickness also decreases. Figure 6 represents the impact of mass transpiration V_c on the temperature profile θ. In both the SWCNTs and MWCNTs cases, temperature decreases concerning V_c. This is because of the way that fluid has a lower thermal conductivity for comprehensive mass transpiration, which

Fig. 8 Skin friction coefficient versus Prandtl number Pr for stretching sheet
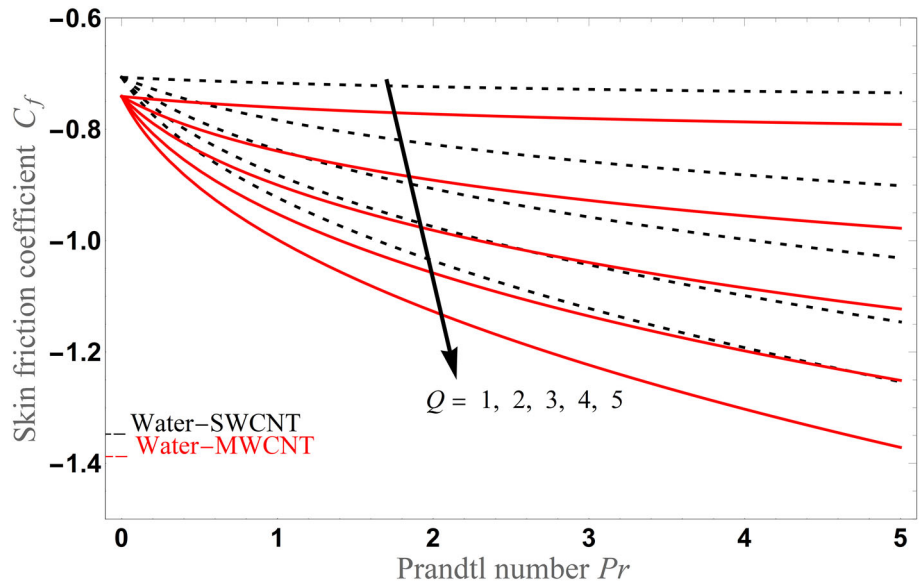
Table 1 Comparison of the present study and related works by other authors

Related works by other authors	Fluids	Value of β
Crane [39]	Newtonian	$\beta = 1$
Pavlov [32]	Newtonian	$\beta = \sqrt{1+M}$
Siddheshwar and Mahabaleshwar [17]	Non-Newtonian	$\beta = \sqrt{\frac{1+M}{(1-k_1)}}$
Siddheshwar et al. [11]	Non-Newtonian	$\beta = \sqrt{\frac{1+M+K}{(1-k_1)}}$
Present work	Non-Newtonian fluid	$f(\eta) = V_c + \Lambda\eta + \frac{D-\Lambda}{\lambda(1+L_1\lambda+L_2\lambda^2)}(1-\exp(-\lambda\eta))$
		$\lambda = \sqrt{\frac{\left(\varepsilon_5+\frac{4}{3}Rd\right)-\Pr\varepsilon_4\varepsilon_3 \pm \sqrt{\left(\left(\varepsilon_5+\frac{4}{3}Rd\right)-\Pr\varepsilon_4\varepsilon_3\right)^2+4\Pr\beta\frac{\varepsilon_1\varepsilon_4\varepsilon_3}{\varepsilon_2}Q\sin^2\tau\left(\varepsilon_5+\frac{4}{3}Rd\right)}}{2\beta\varepsilon_3\left(\varepsilon_5+\frac{4}{3}Rd\right)}},$

(i) The classical Crane [39] flow is recovered from Eq. (21) for $Q = 0$, $\lambda = 1$ and $\tau = 90^0$.

(ii) The classical Pavlov [32] flow is recovered from Eq. (21) for $V_C = 0$, $\lambda = 1$ and.

(iii) Siddheshwar et al. [11] flow is recovered from Eq. (21) for $\lambda = 1$ and $\tau = 90^0$.

lessens conduction and the thickness of the thermal boundary layer, lowering the temperature. It is observed that the temperature and boundary layer density rise in SWCNTs and MWCNTs. When the volume fraction increases, the boundary layer thickness also decreases. Figure 7 portrays the impacts of Prandtl number Pr on the Nusselt number with the variation of mass transportation V_c. It could be seen that the graph of the mass transpiration reduces the thermal layer thickness improving the frequency of heat transfer. When the V_c increases, the extent boundary layer also increases on the stretching/shrinking surface. Additionally, for a given value of Pr, Nu is always higher with multi-wall carbon nanotubes and with single-wall carbon nanotubes. Figure 8 features the skin friction with the variation of Prandtl number Pr for different values of Chandrasekhar's number's Q. The skin friction increments with dense volume fraction and

diminishes with Navier slip because of an increase in carbon nanotube density with solid volume fraction. In effect, one can always find a combination of the governing parameter for which null values either of the skin friction coefficient or the Nusselt number can be obtained, which would convert the sheet either in a frictionless or in an adiabatic wall, respectively (Table 1).

4 Concluding Remarks

A theoretical investigation of the magnetohydrodynamics flow and heat exchange of CNT-based nano-liquid through a variable thicker surface is discussed in this paper. For the suspension of nanoparticles, water is utilized as the base fluid. Saturation in base fluid is accounted for by two types of

CNTs, namely SWCNTs and MWCNTs. This has allowed us to obtain the analytical solution to the problem, explore how the solutions are influenced by the governing physical parameters, and identify the following impacts:

The effects of several parameters on the heat transfer of magnetohydrodynamics Jeffery nanofluid flow of water-based SWCNTs and MWCNTs due to stretching/shrinking surface. The transverse velocity will decrease with an increase in the magnetic constraint in the case of the stretching/shrinking sheet.

The special focus on differences between single- and multi-walled carbon nanotubes in a systematic and qualitative manner.

As Chandrasekhar's number's Q is expanded, multi-wall carbon nanotubes cause an increase in the velocity field relative to multi-wall carbon nanotubes.

For both SMWCNTs and MWCNTs, the temperature profile increases as the radiation estimator is increased.

In the case of the stretching parameter, the dual solution for the skin friction and Nusselt number factors of the carbon nanofluids across the surface is observed to be greater.

This paper is extended to the stability analysis and adding new fluids like ternary fluid and hybrid nanofluid.

This paper is solved analytically, and you can go through this paper to solve numerical method for different cases.

In future, more analytical results are examined along with carbon nanotubes; also, these experiments are examined under different fields like, medicine, engineering, industries, and so on.

References

1. Waqar, A.K.; Culham, R.; Rizwan, U.H.: Heat transfer analysis of Magneto hydrodynamics water functionalized carbon nanotube flow over a static/moving wedge. J. Nanomater. **13**, 934367 (2015)
2. Iijima, S.: Helical microtubules of graphitic carbon. Nature **354**, 56–64 (1991)
3. Baughman, R.H.; Zakhidov, A.A.; De Heer, W.A.: Carbon nanotubes the route toward applications. Science **297**, 787–792 (2002)
4. Nazeer, M., et al.: Multi-phase flow of Jeffrey Fluid bounded within magnetized horizontal surface. Surfaces and Interfaces **22**, 100846 (2021). https://doi.org/10.1016/j.surfin.2020.100846
5. Chu, Y.-M.; Khan, M.I.; Waqas, H.; Farooq, U.; Khan, S.U.; Nazeer, M.: Numerical simulation of squeezing flow Jeffrey nanofluid confined by two parallel disks with the help of chemical reaction: effects of activation energy and microorganisms. Int. J. Chem. Reactor Eng. **19**(7), 717–725 (2021). https://doi.org/10.1515/ijcre-2020-0165
6. Abbas, S.Z.; Nayak, M.K.; Mabood, F.; Dogonchi, A.S.; Chu, Y.; Khan, W.A.: Darcy Forchheimer electromagnetic stretched flow of carbon nanotubes over an inclined cylinder: Entropy optimization and quartic chemical reaction. Math Methods App Sci (2020). https://doi.org/10.1002/mma.6956
7. Hayat, T.; Asad, S.; Alsaedi, A.: Analysis of the flow of Jeffrey fluid with nanoparticles. Chinese Phys. B **24**, 044702 (2015)
8. Turkyilmazoglu, M.: Exact analytical solution for the flow and heat transfer near the stagnation point on a stretching/shrinking sheet in a Jeffery fluid. Int. J. Heat Mass Transfer. **57**, 82–88 (2013)
9. Mahabaleshwar, U.S.; Nagaraju, K.R.; Sheremet, M.A.; Baleanu, D.; Lorenzini, E.: Mass transpiration on Newtonian flow over a porous stretching/shrinking sheet with slip. Chin. J. Phys. **63**, 130–137 (2020)
10. Mahabaleshwar, U.S.; Vinay Kumar, P.N.; Sakanaka, P.H.; Lorenzini, G.: An MHD Effect on a Newtonian Fluid Flow Due to a Superlinear Stretching Sheet. J. Eng. Thermophys. **27**(4), 501–506 (2018). https://doi.org/10.1134/S1810232818040112
11. Siddheshwar, P.G.; Chan, A.; Mahabaleshwar, U.S.: Suction-induced magnetohydrodynamics of a viscoelastic fluid over a stretching surface within a porous medium. IMA J. Appl. Math. **79**, 445–458 (2014)
12. Mahabaleshwar, U.S.; Sneha, K.N.; Huang, H.-N.: An effect of Magnato hydrodynamics and radiation on Carbon nanotubes-Water-based nanofluid due to a stretching sheet in a Newtonian fluid. Case Stud. Therm. Eng. **28**, 101462 (2021)
13. Siddheshwar, P.G.; Mahabaleshwar, U.S.; Andersson, H.I.: A new analytical procedure for solving the non-linear differential equation arising from the stretching sheet problem. Int. J. Appl. Mech. Eng. **18**, 955–964 (2013)
14. Ramesh, B.K.; Shreenivas, R.K.; Achala, L.N.; Bujurke, N.M.: The exact solution of the two-dimensional Magnato hydrodynamics boundary layer flows over a semi-infinite flat plate. Commun. Nonlinear Sci. Numer. Simul. **18**, 1151–1161 (2013)
15. Bujurke, N.M.; Kudenatti, R.B.: Magneto hydrodynamics lubrication flow between rough rectangular plates. Fluid Dyn. Res. **39**, 334 (2007)
16. Mahantesh, M.N.; Vajravelu, K.; Abel, M.S.; Siddalingappa, M.N.: Second-order slip flow and heat transfer over a stretching sheet with non-linear Navier boundary condition. Int. J. Therm. Sci. **58**, 143–150 (2012)
17. Siddheshwar, P.G.; Mahabaleshwar, U.S.: Effects of radiation and heat source on Magneto hydrodynamics flow of a viscoelastic liquid and heat transfer over a stretching sheet. Int. J. Non-Linear Mech. **40**, 807–820 (2005)
18. Mahabaleshwar, U.S.; Vishalakshi, A.B.; Bognar, G.V., et al.: Effect of thermal radiation on the flow of a boussinesq couple stress nanofluid over a porous nonlinear stretching sheet. Int. J. Appl. Comput. Math. **8**, 169 (2022). https://doi.org/10.1007/s40819-022-01355-9
19. Sneha, K.N.; Mahabaleshwar, U.S.; Bennacer, R.; Ganaoui, M.E.L.: Darcy brinkman equations for hybrid dusty nanofluid flow with heat transfer and mass transpiration. Computation **9**, 118 (2021)
20. Khan, M.I.; Khan, S.U.; Jameel, M.; Chu, Y.-M.; Tlili, I.; Kadry, S.: Signifiance of temperature-dependent viscosity and thermal conductivity of Walter's B nanoliquid when sinusodal wall and motile microorganisms density are significant. Surf. Interfaces **22**, 100849 (2021). https://doi.org/10.1016/j.surfin.2020.100849
21. Mahabaleshwar, U.S.; Nagaraju, K.R.; Nadagouda, M.N.; Bennacer, R.; Baleanu, D.: An Magneto hydrodynamics viscous liquid stagnation point flow and heat transfer with thermal radiation & transpiration. J. Therm. Sci. Eng. Progress **16**, 100379 (2020)
22. Anuar, N.S.; Norfifah, B.; Norihan, M.A.; Haliza, R.: Mixed convection flow and heat transfer of carbon nanotubes over an exponentially stretching/shrinking sheet with suction and slip effect. J. Adv. Res. Fluid Mech. Therm. Sci. **59**, 232–242 (2019)
23. Anwar, T.; Kumam, P.; Asifa, K.I.; Phatipha, T.: Generalized unsteady Magneto hydrodynamics natural convective flow of Jeffery model with ramped wall velocity and Newtonian heating: a Caputo-Fabrizio approach. Chin. J. Phys. **59**, 1323 (2020)

24. Khan, W.A.; Khan, Z.H.; Rahi, M.: Fluid flow and heat transfer of carbon nanotubes along with a flat plate with Navier slip boundary. Appl. Nanosci. **4**, 633–641 (2014)

25. Shalini, J.; Manjeet, K.; Amit, P.: Unsteady Magnato hydrodynamics chemically reacting mixed convection nano-fluids flow past an inclined pours stretching sheet with slip effect and variable thermal radiation and heat source. Sci. Direct **5**, 6297–6312 (2018)

26. Yana, S.R.; Mohsen, I.; Mikhail, A.S.; Ioan, I.; Hakan, F.; Oztope, M.A.: Inclined Lorentz force impact on convective-radiative heat exchange of micropolar nanofluid inside a porous enclosure with tilted elliptical heater. Int. Commun. Heat Mass Transfer **117**, 104762 (2020)

27. Anusha, T.; Huang, H.-N.; Mahabaleshwar, U.S.: Two-dimensional unsteady stagnation point flow of Casson hybrid nanofluid over a permeable flat surface and heat transfer analysis with radiation. J. Taiwan Inst. Chem. Eng. **127**, 17 (2021)

28. Anusha, T.; Mahabaleshwar, U.S; Sheikhnejad, Y.: An Magneto hydrodynamics of nanofluid flow over a porous stretching/shrinking plate with mass transpiration and Brinkman ratio. Transport in Porous Media. (2021)

29. Mahabaleshwar, U.S.; Anusha, T.; Sakanaka, P.H.; Bhattacharyya, S.: The impact of inclined Lorentz force and Schmidt number on chemically reactive Newtonian fluid flow on a stretchable surface when Stefan blowing and thermal radiation are significant. Arab. J. Sci. Eng. **46**, 12427 (2021)

30. Hussain, S.; Aly, A.M.; Öztop, H.F.: Magneto-bioconvection flow of a hybrid nanofluid in the presence of oxytactic bacteria in a lid-driven cavity with a streamlined obstacle. Int. Commun. Heat Mass Transfer **134**, 106029 (2022)

31. Selimefendigil, F.; Öztop, H.F.: Thermal management for conjugate heat transfer of curved solid conductive panel coupled with different cooling systems using non-Newtonian power law nanofluid applicable to photovoltaic panel systems. Int. J. Therm. Sci. **173**, 107390 (2022)

32. Pavlov, K.B.: Magnetohydrodynamic flow of an incompressible viscous liquid caused by deformation of plane surface. Magnetnaya Gidrodinamica **4**, 146–147 (1974)

33. Reddy, Y.D.; Goud, B.S.; Nisar, K.S.; Alshahrani, B.; Mahmoud, M.; Park, C.: Heat absorption/generation effect on MHD heat transfer fluid flow along a stretching cylinder with a porous medium. Alexandria Eng. J. **64**, 659–666 (2023). https://doi.org/10.1016/j.aej.2022.08.049

34. Zahor, F.A.; Jain, R.; Ali, A.O.; Masanja, V.G.: Modeling entropy generation of magnetohydrodynamics flow of nanofluid in a porous medium: a review. Int. J. Numer. Methods Heat Fluid Flow. **33**(2), 751–771 (2023). https://doi.org/10.1108/HFF-05-2022-0266

35. Ikram, M.D.; Imran, M.A.; Chu, Y.M.; Akgül, A.: Magneto hydrodynamics flow of a newtonian fluid in symmetric channel with ABC fractional model containing hybrid nanoparticles. Comb. Chem. High Throughput Screen. **25**(7), 1087–1102 (2022)

36. Liaquat, A.L.; Zurni, O.; Sumera, D.; Yuming, C.; Ilyas, K.; Kottakkaran, S.N.: Temporal stability analysis of magnetized hybrid nanofluid propagating through an unsteady shrinking sheet: partial slip conditions. Comput. Mater. Continua **66**(2), 1963–1975 (2021)

37. Rosseland, S.: Astrophysik and atomtheoretische Grundlagen. Springer- Verlag, Berlin (1931)

38. Qureshi, M.A.Z.; Bilal, S.; Chu, Y.-M.; Farooq, A.B.: Physical impact of nano-layer on nano-fluid flow due to dispersion of magnetized carbon nano-materials through an absorbent channel with thermal analysis. J. Mol. Liq. **325**, 115211 (2021). https://doi.org/10.1016/j.molliq.2020.115211

39. Crane, L.J.: Flow past a stretching plate. Z. Angew. Math. Mech. **21**, 645–647 (1970)